JOURNAL OF THE GEOLOGICAL SOCIETY OF JAPAN, Vol. 78, No. 12, p. 677 686, December 1972

NUMERICAL ANALYSIS ON MIGMATITE DOME WITH SPECIAL REFERENCE TO FINITE ELEMENT METHOD

DAIGORO HAYASHI* and KOSHIRO KIZAKI**

(Received May 6, 1972)

Introduction

The numerical treatment of the geological process has recently been advanced in the modern structural geology as well as in the rock mechanics. Since the geological processes, however, are conspicuously slow phenomena and are also involved in complex geological histories, it is required in the numerical analysis carefully to take account of the phenomena and history of the geological structure. If the accurate and substantial understanding of the geological process was lacking, even the most elaborate computations would result in vain. Nevertheless every attempt to clarify a geological process through mathematical means should be tested.

From this point of view, an attempt was made in this paper to analyse the stress distributions within and around a migmatite dome by means of finite element method (F. E. M.). The migmatite dome called the Oshirabetsu dome locates in the southern most part of the Hidaka metamorphic belt, Hokkaido, and its structural analysis has been carried out and the kinematic picture was shown by KIZAKI (KIZAKI, 1956, 1972).

In performing the F. E. M. analysis, it is assumed that the geological materials involving in the analysis are homogeneous and perfectly elastic, although it is certain that the geological rock body must be regarded as visco-elastic body as already mentioned by UEMURA, T. (1971), ITO, H. (1972) and others. This simplification

TECTONIC MAP OF OSHIRABETSU DOME

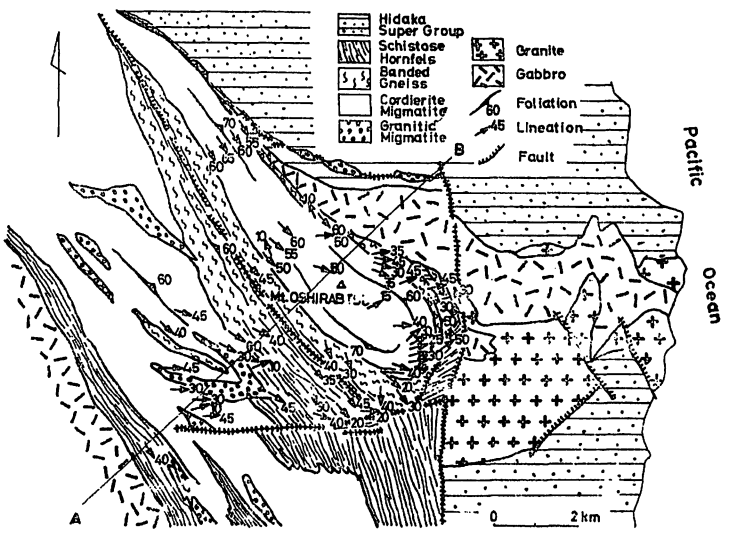

Fig. 1. Tectonic map of the Oshirabetsu dome.

* Department of Mining Engineering, Hokkaido University.
** Department of Geology and Mineralogy, Hokkaido University.

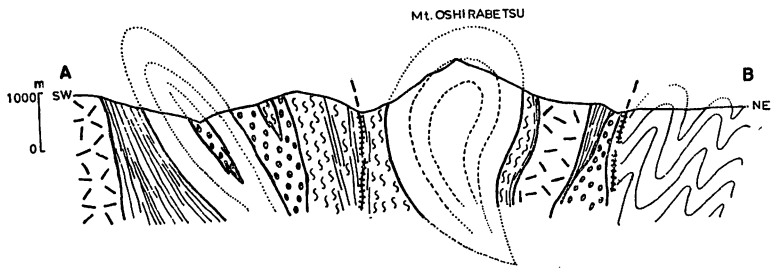

Fig. 2. Cross section of the Oshirabetsu dome.

may make the results differ from the truth on certain points but it would be considered to be an approach to the better understanding of the nature.

Geological Setting of the Oshirabetsu Dome (Fig. 1, 2)

The Oshirabetsu dome locates in the eastern part of the southern extreme region of the Hidaka metamorphic belt and shows a characteristic shape like "Falling star" the main portion of which is regarded as a dome. The core portion of the dome is composed mainly of cordierite migmatite and surrounded by banded biotite gneiss. The dome 3 km wide at the main portion, extends to north-west forming the trail of the "Falling star" which reduces the width out within 10 km with monoclinic inclination to east.

A gabbro body on the north-eastern side of the dome, separates the biotite hornfels zone distributed outside. The linear arrangement of small granitic migmatite sheets occurs along the sheared zone in the hornfels aureole. On the eastern side of the dome, the gabbro and granite bodies are separated by schistose biotite hornfels accompanied with sheared zone and thrust fault. To the south-west, the schistose biotite hornfels, ban ded biotite gneiss and cordierite migmatite which are separated by sheared zone from the "Falling star" are among the other tectonic units of the core of the Hidaka metamorphic belt on the south-western side.

The structural study of the Oshirabetsu dome with special reference to petrofabric analysis has been carried out and the three dimensional comparative structural study has been published (KIZAKI, 1956, 1972). According to the comparative study of the Oshirabetsu dome and Pipairo complex (op. cit.), three dimensional form of the "Falling star" is clearly shown (KIZAKI, 1972). However, in the present study, the two dimensional vertical section of the main portion of the "Falling star" is treated for the analysis of stress distribution because of the simplification of the computation for the first step.

Brief Note on the Finite Element method

The finite element method, based on the principle of virtual work, shall be briefly described. A vertical plane which is cut through the Oshirabetsu dome along A–B line was chosen as shown in Figure 2, and the plane is divided into 668 finite-elements of triangle (Fig. 5). For a typical element (Fig. 3), assuming homogeneous stress within the element, the vector of nodal displacements $\mathbf{u}^e$ and the vector of nodal forces $\mathbf{F}^e$ can be expressed in matrix form as;

$$\mathbf{u}^e=\begin{Bmatrix}\mathbf{u}_1\\ \mathbf{u}_2\\ \mathbf{u}_3\end{Bmatrix}=\begin{Bmatrix}u_{1x}\\ u_{1y}\\ u_{2x}\\ u_{2y}\\ u_{3x}\\ u_{3y}\end{Bmatrix},\quad \mathbf{F}^e=\begin{Bmatrix}\mathbf{F}_1\\ \mathbf{F}_2\\ \mathbf{F}_3\end{Bmatrix}=\begin{Bmatrix}F_{1x}\\ F_{1y}\\ F_{2x}\\ F_{2y}\\ F_{3x}\\ F_{3y}\end{Bmatrix}\quad\cdots(1)$$

By continuity of displacement within the element and with adjacent element, a displacement function of two linear polynomials can be chosen for the case of two dimensions. So it can be represented as follows;

$$\mathbf{u}=\begin{Bmatrix}u_x\\ u_y\end{Bmatrix}=\begin{bmatrix}a_0 & a_1 & a_2\\ b_0 & b_1 & b_2\end{bmatrix}\cdot\begin{Bmatrix}1\\ x\\ y\end{Bmatrix}\quad\cdots\cdots\cdots(2)$$

$\mathbf{u}$: inner displacement vector

Eq. (2) may be written in the form as;

$$\mathbf{u}=\begin{bmatrix}1 & x & y & 0 & 0 & 0\\ 0 & 0 & 0 & 1 & x & y\end{bmatrix}\cdot\begin{Bmatrix}a_0\\ a_1\\ a_2\\ b_0\\ b_1\\ b_2\end{Bmatrix}=[R']\cdot\alpha\quad\cdots(3)$$

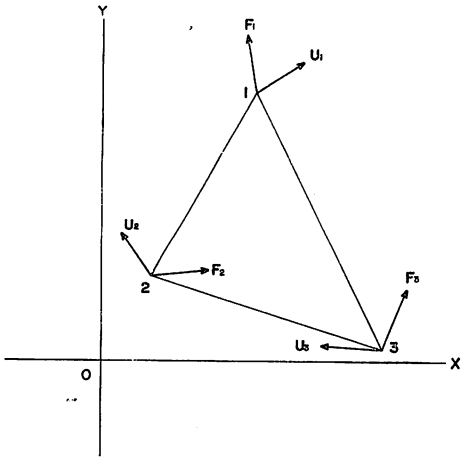

Fig. 3. A triangle finite-element which is optionally selected among the divided finite-elements (See text).

Therefore the vector of nodal displacement is listed as a product of matrix and vector.

$$\mathbf{u}^e=\begin{Bmatrix}R_1\\R_2\\R_3\end{Bmatrix}\cdot\alpha=[R]\cdot\alpha \quad \cdots\cdots(4)$$

[R]: shape function matrix; α: generalized displacement vector

Using x_i and y_i for the x- and y-coordinate at a nodal point i, the shape function matrix $[R_i]$ at the point is represented by;

$$[R_i]=\begin{bmatrix}1 & x_i & y_i & 0 & 0 & 0\\ 0 & 0 & 0 & 1 & x_i & y_i\end{bmatrix}\ (i=1,2,3)\cdots(5)$$

From Eq. (4) the generalized displacement vector α are given by;

$$\alpha=[R]^{-1}\cdot\mathbf{u}^e \quad \cdots\cdots(6)$$

Using Δ for $\det\begin{bmatrix}1 & x_1 & y_1\\1 & x_2 & y_2\\1 & x_3 & y_3\end{bmatrix}$, the inverse matrix $[R]^{-1}$ will be expressed;

$$[R]^{-1}=\frac{1}{\Delta}\begin{pmatrix}\Delta_{11} & 0 & \Delta_{21} & 0 & \Delta_{31} & 0\\ \Delta_{12} & 0 & \Delta_{22} & 0 & \Delta_{32} & 0\\ \Delta_{13} & 0 & \Delta_{23} & 0 & \Delta_{33} & 0\\ 0 & \Delta_{11} & 0 & \Delta_{21} & 0 & \Delta_{31}\\ 0 & \Delta_{12} & 0 & \Delta_{22} & 0 & \Delta_{32}\\ 0 & \Delta_{13} & 0 & \Delta_{23} & 0 & \Delta_{33}\end{pmatrix}\quad\cdots\cdots(7)$$

Where Δ equals to two times area of the triangle element, and Δ_{ij} is the cofactor of i, j-components of Δ, for example, $\Delta_{23}=-\det\begin{bmatrix}1 & x_1\\1 & x_3\end{bmatrix}$ Consequently, from Eq. (3) and Eq. (6) the inner displacement of the triangle is equated as follows;

$$\mathbf{u}=[R']\cdot\alpha$$
$$=[R']\cdot[R]^{-1}\cdot\mathbf{u}^e \quad \cdots\cdots(8)$$

Now strain vector $\mathbf{e}$ is represented;

$$\mathbf{e}=\begin{Bmatrix}\varepsilon_x\\\varepsilon_y\\\gamma_{xy}\end{Bmatrix}=\begin{Bmatrix}\dfrac{\partial u_x}{\partial x}\\[2mm]\dfrac{\partial u_y}{\partial y}\\[2mm]\dfrac{\partial u_x}{\partial y}+\dfrac{\partial u_y}{\partial x}\end{Bmatrix}$$
$$=\begin{bmatrix}0&1&0&0&0&0\\0&0&0&0&0&1\\0&0&1&0&1&0\end{bmatrix}\cdot\alpha=[B]\cdot\alpha$$
$$=[B]\cdot[R]^{-1}\cdot\mathbf{u}^e \quad \cdots\cdots(9)$$

Where the matrix [B] is called the strain-generalized displacement matrix and its components are not functions of variables x and y, so that one can see that the strain is constant in each element.

The relation of stress vector $\mathbf{p}$ and strain vector $\mathbf{e}$ is;

$$\mathbf{p}=\begin{Bmatrix}\sigma_x\\\sigma_y\\\tau_{xy}\end{Bmatrix}$$
$$=\frac{E(1-\nu)}{(1+\nu)(1-2\nu)}\begin{pmatrix}1 & \dfrac{\nu}{1-\nu} & 0\\[2mm]\dfrac{\nu}{1-\nu} & 1 & 0\\[2mm]0 & 0 & \dfrac{1-2\nu}{2(1-\nu)}\end{pmatrix}\cdot\mathbf{e}$$
$$=[K]\cdot\mathbf{e} \quad \cdots\cdots(10)$$

Where ν is the POISSON's ratio, E the YOUNG's modulus and [K] is the stress-strain matrix. Eq. (10) is valid for the case of plane strain.

Let the virtual displacement be $\mathbf{u}^{*e}$ when the element is deformed, the strain energy U of this element is given by;

$$U=\int_V(\mathbf{e}^*)^T\cdot\mathbf{p}\,dV$$
$$=\int_V(\mathbf{e}^*)^T\cdot[K]\cdot\mathbf{e}\,dV$$
$$=\int_V(\mathbf{u}^{*e})^T\cdot([R]^{-1})^T\cdot[B]^T\cdot[K]\cdot[B]\cdot[R]^{-1}\cdot\mathbf{u}^e\,dV$$
$$=\int_V(\mathbf{u}^{*e})^T\cdot[B^*]^T\cdot[K]\cdot[E^*]\cdot\mathbf{u}^e\,dV$$

Where $[B^*]$ is equal to $[B]\cdot[R]^{-1}$ and $\mathbf{e}^*$ is the vector of virtual strain.

As the nodal forces are already defined by Eq. (1), the external work W is:

$$W=(\mathbf{u}^{*e})^T\cdot\mathbf{F}^e$$

And the strain energy is equal to the external work, so that the following equation holds.

$$(\mathbf{u}^{*e})^T\cdot\mathbf{F}^e=\int_V(\mathbf{u}^{*e})^T\cdot[B^*]^T\cdot[K]\cdot[B^*]\cdot\mathbf{u}^e\,dV$$
$$=(\mathbf{u}^{*e})^T\cdot\left\{\int_V[B^*]^T\cdot[K]\cdot[B^*]\,dV\right\}\cdot\mathbf{u}^e$$

While the vector of nodal force is represented by;

$$\mathbf{F}^e=\left\{\int_V[B^*]^T\cdot[K]\cdot[B^*]\,dV\right\}\cdot\mathbf{u}^e$$

Now, the stiffness equation is obtained.

$$\mathbf{F}^e=[A]\cdot\mathbf{u}^e$$

Where $[A]$ is called the stiffness matrix and can be written in the form;

$$[A]=\int_V[B^*]^T\cdot[K]\cdot[B^*]\,dV$$

In this case, each matrix is constant in the element, then the product of matrices i. e. $[B^*]^T\cdot[K]\cdot[B^*]$, is constant. Consequently, it is possible to take off the integral mark,

$$[A]=[B^*]^T\cdot[K]\cdot[B^*]\cdot V$$

Where V is the volume of the element.

By solving the above stiffness matrix, one can get undecided nodal forces and nodal displacements for every element. Furthermore, using these nodal displacements, the values of stress and strain could be obtained.

Further and detailed discussions on the F. E. M. are referred to such publications as ZIENKIEWICZ *et al.* (1967) and FUJII (1970) and so forth.

Modelling and Conditions for Analysis

In order to determine the stress field during the upward motion of the migmatite dome, it is assumed that the Oshirabetsu dome has been developed by the difference of the density between the migmatite and the country rocks during the later stage of the Hidaka orogeny. It could be considered that the upward motion of the granitic rocks within the gravity field would possibly bring about the mountain building.

The plane on the A–B section (Fig. 2) was selected for the analysis and the following conditions were assumed.

(1) State is "Plane Strain" on the A–B section and the composed rocks are perfectly elastic and isotropic in all directions.

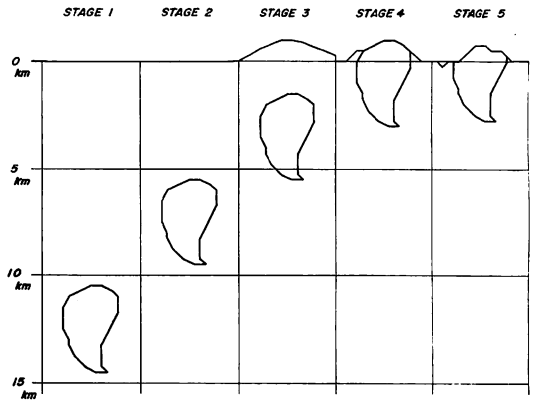

Fig. 4. Models to be divided into the five assumed stages in order to analyse. The dome is composed of cordierite migmatite and its neighbouring portion is composed of massive hornfels. At the Stages 1 and 2, the surface is assumed to be flat, at the Stages 3, 4 and 5 the surface to be convex.

(2) There are two rock species i.e. cordierite migmatite and massive hornfels.

(3) Gravity is only considered as the external force.

This means that there had been no tectonic forces in this area through all the stages.

The models for numerical analysis are divided into five stages as follows; (Fig. 4)

Stage 1: The Oshirabetsu dome had been situated at the depth of 10.5 to 14.5 km below the surface,

Stage 2: The dome had been situated at the depth of 5.5 to 9.5 km below the surface.

Stage 3: The dome had been lifted almost to the surface and the hornfels covering had been eroded away, then the surface over the upper part of the dome had been formed into the mountain ridge.

Stage 4: The upper part of the dome had been exposed.

Stage 5: Present stage.

For the purpose of the F.E.M. analysis, the section of the Oshirabetsu dome and its neighbouring portion are divided into 668 elements on the A–B section. Figure 5 indicates the partition, external force boundary condition and displacement boundary condition. Table 1 indicates the physical constants used for the calculation.

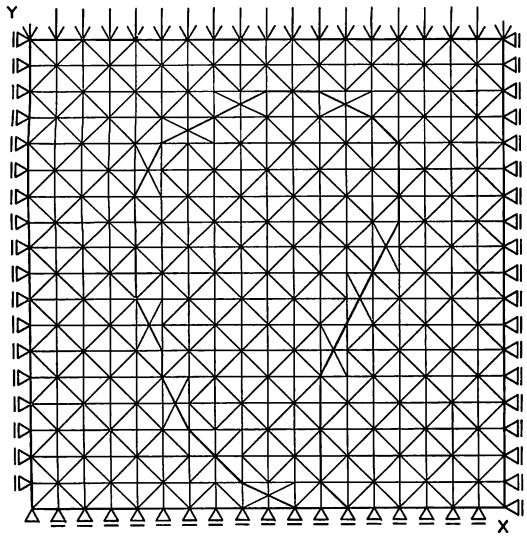

Fig. 5. Partition on the A–B section, which indicates the 668 divided finite-elements of triangle. Using next symbols, the external force boundary condition and displacement boundary condition are indicated.

△: Symbol at which point it is forbidden to move to all directions.

△: Symbol at which point displacements along horizontal line are only permitted.

|▷, ◁|: Symbol at which point displacements along vertical line are only permitted.

↓: Symbol which indicates the direction of load caused the weight of the upper part.

Results of Analysis

Under these conditions as described above, the data were analysed with the computer of Hokkaido University Computing Centre (FACOM 230—60), and then the next five results are obtained.

(1) Principal stresses are all compressive in the whole area through all the stages.

(2) Absolute values of principal stresses are about two times greater in the portion of massive hornfels than in that of cordierite migmatite.

(3) Absolute value of every principal stress is revealed to be within the elastic region decided by thermal-triaxial compressive experiment.

(4) Directions of the principal stresses are generally constant during all stages only under the gravity field condition.

(5) Foliations are situated to be normal to the resultant stresses (compressive) acting on the foliations.

Table 1*. Physical constants used for the calculation and failure strengths of the rocks, which were given by the uniaxial compressive test at normal temperature (20—30°C) and normal pressure (1 atm).

	ρ (g/cm³)	E (kb)	ν	Sc (kb)	Ss (kb)
m. Hf.	3.04 0.10	304 58	0.40 0.01	1.81 0.49	0.21
c. M.	2.76 0.02	176 62	0.36 0.02	0.95 0.36	0.12

ρ: density, E: YOUNG's modulus, ν: POISSON's ratio (dynamic), Sc: compressive strength, Ss: shearing strength. m. Hf.: massive hornfels and c.M.: cordierite migmatite. The average values of each item are indicated at the upper line and their standard deviations except for the item of Ss are shown at the lower line. (HAYASHI, 1971)

* The data of thermal-triaxial compressive constants for the rocks around Oshirabetsu are not obtained yet.

And in the present paper, according to elasticity, E and ν are used to be constant.

Discussions

The stress distribution at every stage, which are represented by the principal stresses (σ_1, σ_2) in the triangle domain, along the boundary between cordierite migmatite and massive hornfels, are shown in Figures 6—10.

The values of the principal stresses are negative on all stages, that is, the principal stresses are compressive.

For the sense of absolute value, the greater one was named the maximum principal stress (σ_1), and the other the minimum principal stress (σ_2).

In every figure (Figs. 6—10), each pair of lines, which are perpendicular each other and whose lengths indicate the absolute values, represents the maximum principal stress (σ_1) and the minimum principal stress (σ_2) of the respective triangle. The intersections of σ_1 and σ_2 selected conventionally to be the centres of the gravity of the triangle elements. The directions of principal stresses in the Stage 1 and 2 are exactly identical, and also those in the Stage 3, 4 and 5 are roughly identical to these figures, though these are obvious from the boundary conditions.

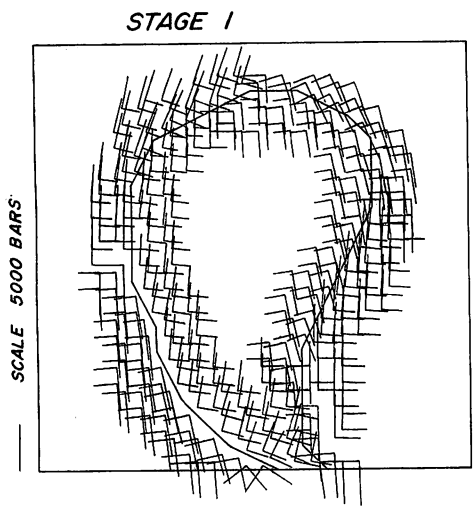

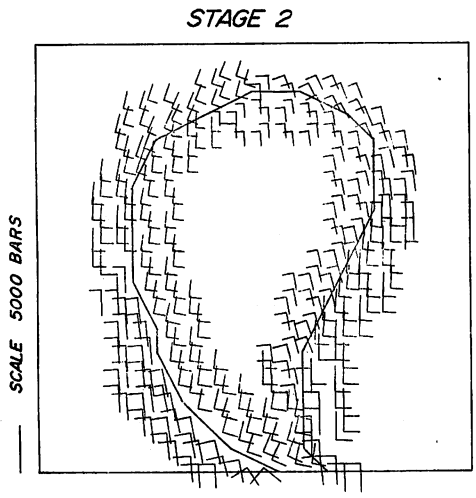

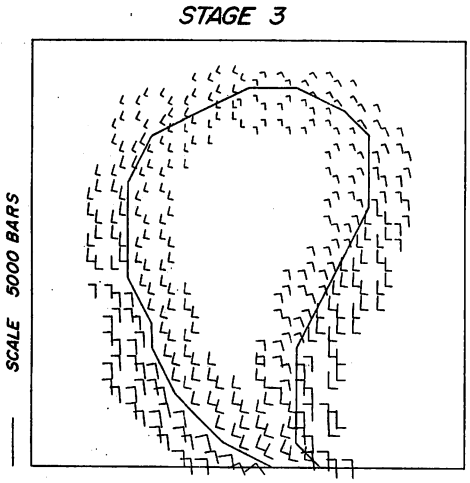

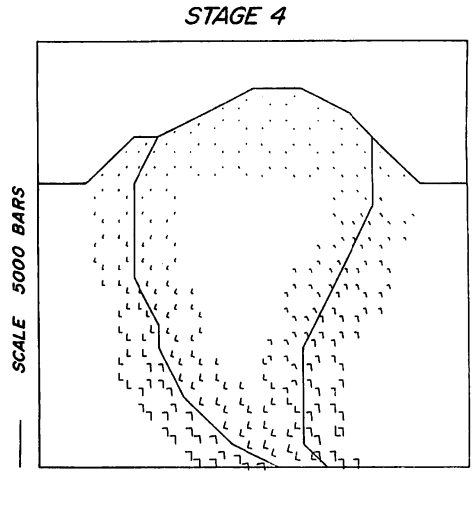

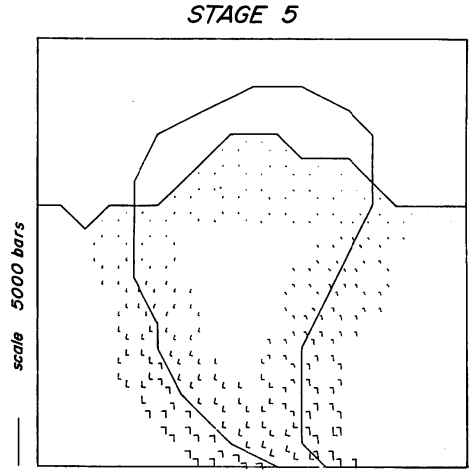

Figs. 6—10. Stress distribution around the boundary of the dome at every stage. The stress distributions at the core portion and also the external area of the dome are eliminated in the figures because the directions of stress vectors are constant through the stages. They are shown on the part around the boundary. Every pair of perpendicular lines represents σ_1 (long line) and σ_2 (short line) at each intersection. The length of every line indicates the absolute value (all compressive).

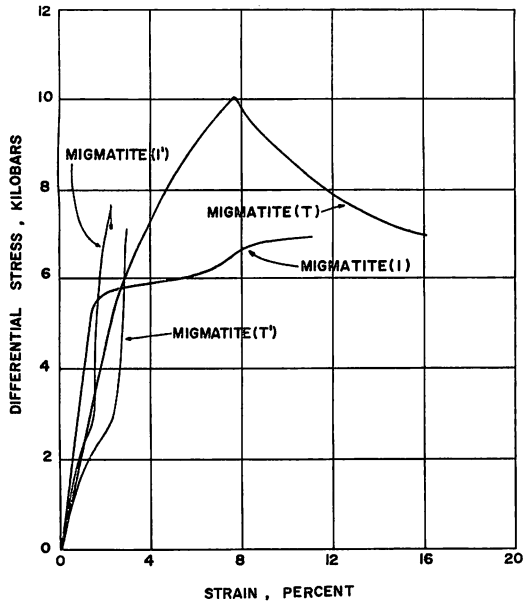

Fig. 11. Stress-strain curve of the thermal-triaxial compressive experiment using migmatite by BORG I. and HANDIN J. (1966).
Confining pressure: 5 kb, Temperature: 500°C.
Migmatite(T): Migmatite which is loaded normal to foliation.
Migmatite(l): Migmatite which is loaded parallel to foliation.
Migmatite(T') and (l') were given at 1 kb and 150°C.
From the figure, the stress-strain curves from the state at 150°C–1 kb to 500°C–5 kb would be considered to lie in the middle region between them.

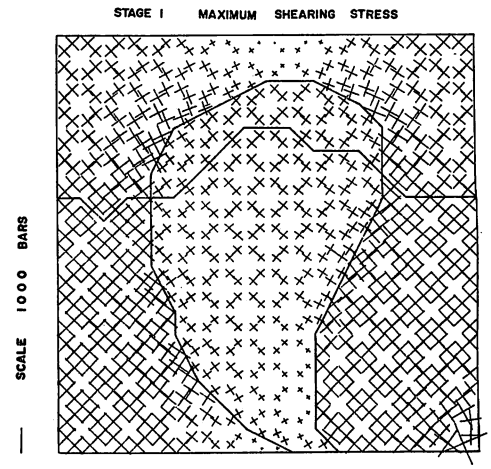

Fig. 12. Shearing stress distribution on the region (334 points) at the Stage 1. Every crossed line represents conjugated shearing stress at each intersection. The figure indicates the outline of the dome and the present eroded shape.

Therefore, if these boundary conditions had not changed greater, it should be safe to conclude that the stress field around the Oshirabetsu dome would have been generally constant through all the stages.

The figures clearly show that the absolute values of principal stresses (σ_1, σ_2) are about two times greater in the part of massive hornfels than in that of cordierite migmatite. It is caused by the difference of their YOUNG's modulus.

As the result of the calculations and comparative study to the thermal-triaxial compressive experiments using migmatite by BORG and HANDIN (1966) (Fig. 11), the values of principal stresses of the rocks are revealed to be within the elastic region (maximum value of all principal stresses through all stages is 5.15 Kb which is the value of σ_1 at Stage 1) so that the failure should not take place so far as the present scale of the triangle is concerned. As a matter of course, it does not mean that in this area the failures had not brought about, because the gravity had only been assumed for the force in the calculation.

The failures should take place at first along the boundary of the two rock species by the stress concentration. It may be represented by the foliation of the gneiss which surrounds the dome as a narrow belt. Another possibility of the failure could be the sheared zones which occur outside of the dome.

However, it is hardly considered that the failures had formed the present sheared zones by the stress concentration of the scale mentioned above. Consequently, it should be considered that the other forces besides gravity e.g. forces caused by the tangential stress, have been acting in this area.

Now, from the next simple equation the values of maximum shearing stresses (τ_{max}) are calculated in each domain, and the directions of τ_{max} have forty five degrees from each principal axis.

$$\tau_{max} = \frac{\sigma_1 - \sigma_2}{}$$

On the 12, each crossed line indicates the value and direction of τ_{max} at the Stage 1. This figure shows that the directions of τ_{max} are parallel to some parts of the curved outline of

the dome and that the directions of σ_1 and σ_2 are parallel to the boundaries of the other parts of the dome (Figs. 6, 7, 8, 9, 10 and 12).

Now, though the analysis is carried out for the two dimensional situation, it is able to obtain the values of the third principal stresses σ^*, which are perpendicular to the A–B section, using the next equations.

$$\sigma^* = \frac{\nu(1-\nu)}{(1+\nu)(1-2\nu)}(\sigma_1+\sigma_2)$$

In this case, the stresses σ^* are identified with σ_3, because that the absolute values of σ^* are less than those of σ_1 and σ_2 (ref. Table 2). Using this equation, the values of σ_3 are calculated on the domains, on which the values of σ_θ and τ_θ are calculated, and indicated on the Table 2.

On the Formation of Foliation

From the values and directions of principal stresses, the normal stresses (σ_θ) and shearing stresses (τ_θ) on the fifteen boundaries, which are placed between cordierite migmatite and massive hornfels, can be calculated by the next relations,

$$\sigma_\theta = \frac{\sigma_1+\sigma_2}{2} + \frac{\sigma_1-\sigma_2}{2}\cos 2\theta$$

$$\tau_\theta = -\frac{\sigma_1-\sigma_2}{2}\sin 2\theta$$

where θ is the angle between the horizontal line

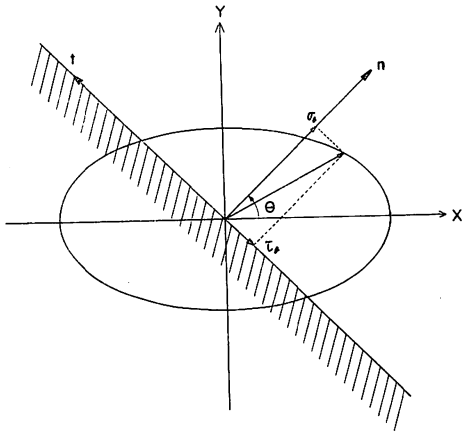

Fig. 13. Stress ellipse shows the relation between the resultant and principal stresses. The resultant stress acts on a spontaneous plane, and is composed of normal stress and shearing stress. The vector **n** is the normal vector of the spontaneous plane and the vector **t** is the unit vector to be perpendicular to **n**.

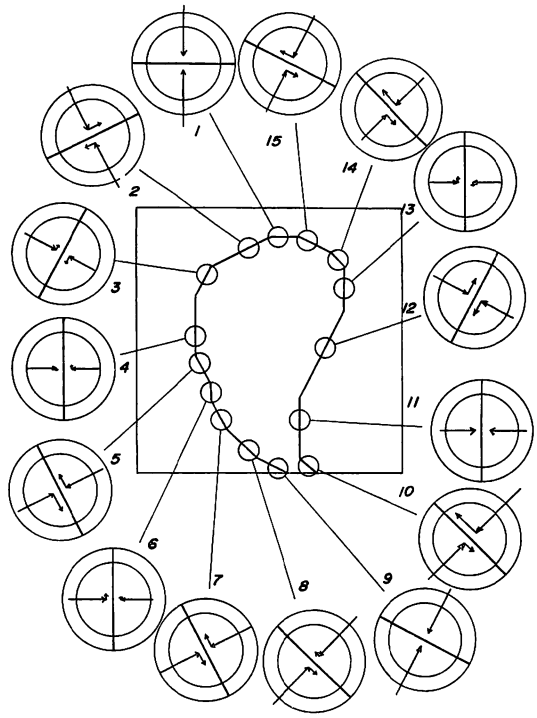

Fig. 14. The normal stresses and shearing stresses on the fifteen boundaries of the dome which in fact are deformed but for the simplification are regarded as pre-deforming one. The inner circle indicates the value of 1 kb and the outer that of 1.5 kb.

and each boundary. On the Figure 13, **n** is the unit vector which is normal to the boundary and **t** is the unit vector perpendicular to **n**. The relations between their components and θ are decided as follows.

$$\mathbf{n} = \begin{Bmatrix} n_1 \\ n_2 \end{Bmatrix}, \quad \mathbf{t} = \begin{Bmatrix} t_1 \\ t_2 \end{Bmatrix}, \quad \begin{cases} n_1 = t_2 = \cos\theta \\ n_2 = -t_1 = \sin\theta \end{cases}$$

The fifteen boundaries in question are parallel to the trace of foliations on the A–B section. Calculated values of σ_θ and τ_θ on the Stage 1 are shown in Table 2 and they are illustrated in Figure 14, in this case each pair of resultant stresses on a certain boundary is different in the absolute value as well as in the direction respectively, because in the analysis using the F.E.M. the constitutive equation does not hold and also the boundaries for which the pre-deformed boundaries are used, are deformed in fact.

From the Figure 14, it is clear that the foliation tends to be perpendicular to the resultant stress.

Table 2. Calculated values of σ_1, σ_2, σ_3, σ_θ and τ_θ, where σ_1 is the maximum principal stress, σ_2, the minimum principal stress, σ_3, the principal stress to be normal to the A–B plane, σ_θ and τ_θ are the normal stress and shearing stress on each boundary respectively. Nb is the boundary number, Ne, the number of element and θ is the angle between the horizontal line and each boundary. (See text. & Fig. 14)

Nb	Ne	σ_1 (kb)	σ_2 (kb)	σ_3 (kb)	θ (deg)	σ_θ (kb)	τ_θ (kb)
1	577	−2.82946	−1.81332	−0.39327	0.0	−1.922	−0.035
	615	−2.94871	−2.36217	−0.45522		−1.765	−0.053
2	573	−2.90379	−1.79869	−0.39832	26.5	−1.786	0.437
	571	−3.16793	−2.21976	−0.46180		−1.583	0.474
3	492	−2.76574	−1.86550	−0.39229	63.5	−1.045	0.297
	491	−4.29252	−2.27218	−0.56269		−1.155	0.184
4	343	−2.97331	−2.01608	−0.42263	90.0	−1.023	−0.115
	342	−4.61914	−2.06138	−0.57261		−1.032	−0.052
5	269	−3.19105	−2.02845	−0.44212	−63.5	−1.364	−0.532
	268	−4.60907	−2.27877	−0.59038		−1.383	−0.711
6	195	−2.91311	−2.14880	−0.42877	90.0	−1.087	−0.094
	194	−4.69676	−2.49768	−0.61666		−1.264	0.173
7	123	−3.19273	−2.24895	−0.46094	−63.5	−1.455	−0.450
	122	−4.53189	−2.71795	−0.62141		−1.480	−0.453
8	54	−3.16719	−2.36605	−0.46869	−45.0	−1.919	−0.216
	53	−4.07748	−3.18156	−0.62220		−1.827	−0.394
9	22	−3.15436	−2.52811	−0.48133	−26.5	−1.889	−0.005
	21	−3.62619	−3.41329	−0.60338		−1.711	−0.026
10	25	−3.21192	−2.27510	−0.46478	−45.0	−1.776	−0.435
	26	−4.85300	−2.88932	−0.66363		−2.203	−0.955
11	133	−2.81669	−2.44252	−0.44548	90.0	−1.225	0.034
	134	−4.23633	−2.50482	−0.57781		−1.253	−0.022
12	323	−3.11029	−1.96491	−0.42990	63.5	−1.439	0.560
	324	−4.15950	−2.25051	−0.54943		−1.337	0.598
13	473	−2.84548	−1.84827	−0.39758	90.0	−0.963	0.191
	474	−4.46609	−1.96722	−0.55142		−1.008	0.239
14	547	−2.84442	−1.67766	−0.38304	−45.0	−1.218	−0.545
	548	−4.17937	−2.06818	−0.53550		−1.313	−0.713
15	581	−2.80477	−1.75119	−0.38591	−26.5	−1.625	−0.475
	582	−3.37669	−2.27554	−0.48448		−1.561	−0.534

It seems, therefore, to be reasonable that the foliation, especially in the gneiss and migmatite and other extremely deformed rocks, may be resulted from as to be normal to the compressive force during the upward movement of the dome.

Though the shape of the dome could have been deformed through the upward movement so that the stress conditions are changeable, the shearing stresses works strongly on the more curved bounderies (2, 5, 7, 10, 12, 14, 15 in the Fig. 14). It is reasonable from the observations in the field that the intense foliations are developed on the parts.

The values of the shearing stresses are shown in Table 2 and Figure 14, and there are some portions without or with very weak shearing stress.

Postscript and Acknowledgements

This analysis is calculated under the perfect elastic state, so that it means that the stress field obtained above is the momentary one during the uplift of the dome. Therefore, the continuous variations of the stress conditions through the time passed could not be obtained. This variation is, however, very important in the geological view point and is clear that this would be verified by the hypothesis regarding rocks as visco-elastic body, for example, as MAXWELL body for the first step.

The authors thank Professor S. KINOSHITA of the University of Hokkaido who carefully reviewed the manuscript and Lecturer S. YAMASHITA who kindly permitted to use the program of the F. E. M. They are also grateful to Mr. YOSHIDA for preparing the figures and to Mr. TANAKA, Mr. MATSUDA and Mr. SHIRAISHI for their useful discussions.

References

BORG, I. & HANDIN, J. (1966), Experimental deformation of crystalline rocks. *Tectonophysics*, vol. 3, p. 249—368.

FUJII, K. (1970), Structural analysis by finite element method. *Chikyu Kagaku (Earth Science)*, vol. 24, p. 193—200.

HAYASHI, D. (1971), The geology around Toyonidake, in the Southern Hidaka Belt, Hokkaido and the mechanical properties of rocks, graduate thesis, unpublished.

ITO, H. (1972), Change of topography due to flow of the crust under the condition of isostasy. *Jour. Geol. Soc. Jap.* vol. 78, p. 29—38.

KIZAKI, K. (1956), Petrofabrics of the Oshirabetsu migmatite dome in the southern region of the Hidaka Metamorphic Zone, Hokkaido. *Jour. Geol. Soc. Jap*, vol. 62, p. 415—430.

KIZAKI, K.(1972), Configuration of migmatite dome. *Jour. Fac. Sci. Hokkaido Univ.*, Ser. IV vol. XV, p. 157—172.

UEMURA, T. (1971), Some problems on tectonic flow of rocks. *Jour. Geol. Soc. Jap.*, vol. 77, p. 273—278.

ZIENKIEWICZ, O. C. & CHEUNG, Y. K. (1967), The finite element method in structural and continuum mechanics. McGraw-Hill Publishing Co. LTD., England.

有限要素法によるミグマタイトドームの数値解析

林　大五郎・木崎　甲子郎

(要　旨)

現在の地質学によると，花崗岩質岩体の上昇運動は周囲岩体との密度の差による事がひとつの原因である，と考えられている．この小論は，密度の差による花崗岩質岩体の浮上中の応力場の変遷を論じたものである．この目的のため，すでに木崎（1956, 1972）によって詳細な構造解析の行なわれている，日高変成帯最南端部「音調津ミグマタイトドーム」をフィールドとして選んだ．木崎によって得られた構造解析データをすべて考慮することは，現在では不可能であるため，つぎの単純化を行なった．1）岩石種は二種（菫青石ミグマタイト，塊状ホルンフェルス）とする．2）それらは完全弾性体である．3）重力のみを仮定した平面歪状態（音調津山地山頂を含む NE—SW 方向の垂直断面内において）と考える．本解析は次の五つの場合を仮定し，それぞれについて行なわれた．ドームが，地表下 10.5～14.5km（この場合地表は平坦であるとする），5.5～9.5km（同様），2.5～6.5km（地表は山型に盛り上がっているとする）等の深さにある場合，更にドームが地表へ露出した場合，そして削剝された場合（現在）の以上五段階である．このような仮定のもとに解析した結果，つぎの結論を得た．1）主応力は全段階を通じ，かつ解析領域全般にわたってすべて圧縮性である．2）ドーム内部の主応力値はドーム外部のそれの約半分である．3）すべての主応力の絶対値は加熱—三軸圧縮実験によって決定された弾性領域の範囲内にある．4）主応力の方向は全段階を通じてほぼ一定している．5）フォリエーション面に働く合応力の方向はほとんどその面に垂直である，すなわち合応力はほとんどフォリエーションに対して垂直応力成分からなっている．

地　名

Oshirabetsu　音調津，　Pipairo　ピパイロ

ERRATA

Vol. 78, No. 12, p. 677—686, 1972.

Daigoro HAYASHI and Koshiro KIZAKI: Numerical Analysis on Migmatite Dome with Special Reference to Finite Element Method.

	Incorrect	Correct
p. 683	$\tau_{max}= \sigma_1-\sigma_2$	$\tau_{max}=\frac{\sigma_1-\sigma_2}{2}$
	On the 12,	On the Figure 12,
p. 684	$\sigma^*= \nu(1-\nu) \quad (\sigma_1+\sigma_2)$	$\sigma^*=\frac{\nu(1-\nu)}{(1+\nu)(1-2\nu)}(\sigma_1+\sigma_2)$
	In this σ^* are	In this case, the stresses σ^* are